Supplementary information

Electron Dynamics in Plamons

Do Thi Bich Hue, [a,b] Ding Wen Jun, [c] Zackaria Mahfoud, [d] Wu Lin*[c] and Michel Bosman*[a,d]

[a] *Department of Materials Science and Engineering, National University of Singapore, 9 Engineering Drive 1, Singapore, 117575. E-mail: msemb@nus.edu.sg*
[b] *NUS Graduate School for Integrative Sciences and Engineering, National University of Singapore, 21 Lower Kent Ridge, Singapore, 119077.*
[c] *Institute of High Performance Computing, Agency for Science, Technology, and Research (A*STAR), 1 Fusionopolis Way, 16-16 Connexis, Singapore, 138632. Email: wul@ihpc.a-star.edu.sg*
[d] *Institute of Materials Research and Engineering, Agency for Science, Technology and Research (A*STAR), 2 Fusionopolis Way, Singapore, 138634*

Contents

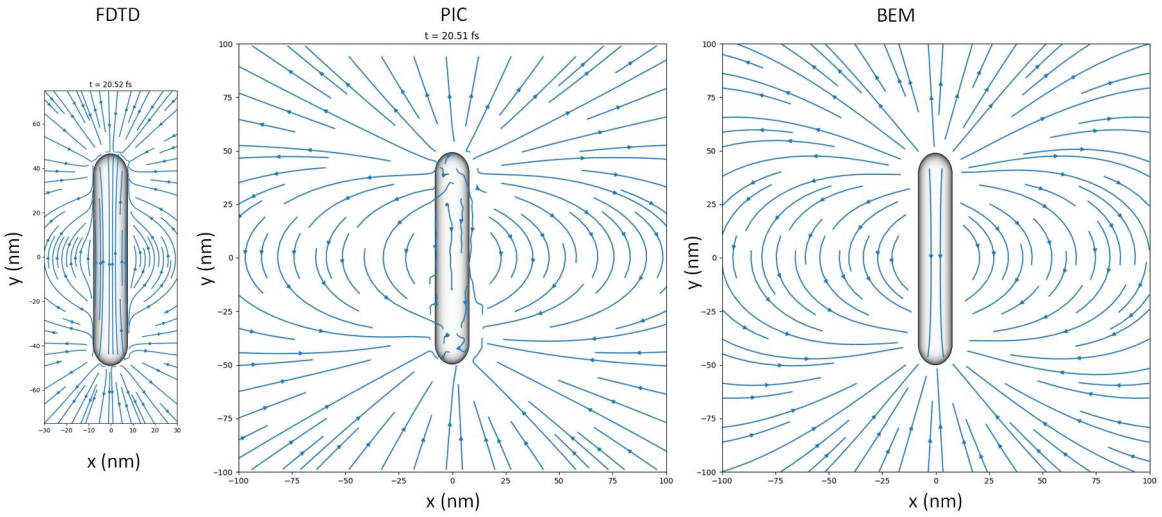

Figure S1. Electric field lines calculated by Particle-in-Cell for plasmons (PIC), by the boundary element method (BEM) and by the finite-difference time-domain (FDTD) method. The same Au nanorod was simulated, with length 100 nm and width 20 nm. In PIC and FDTD, the nanorod is excited at its resonance frequency for 10 fs, then allowed to dampen out. In FDTD, the dielectric function of Au is taken from the Drude's plasma model with the plasma frequency $\omega_p = 1.377 \times 10^{16}\ rad/s$ and $\gamma = 7.143 \times 10^{13}\ rad/s$. The FDTD map is smaller due to the smaller monitor size set. In BEM, the nanorod is simulated with the Au dielectric function from Johnson and Christy[1]. For all maps, the E_x and E_y field are plotted on the $z = 0$ plane of symmetry. The PIC and FDTD maps are plotted during damping after excitation has ended. The BEM map is plotted from the imaginary part of E_x and E_y.

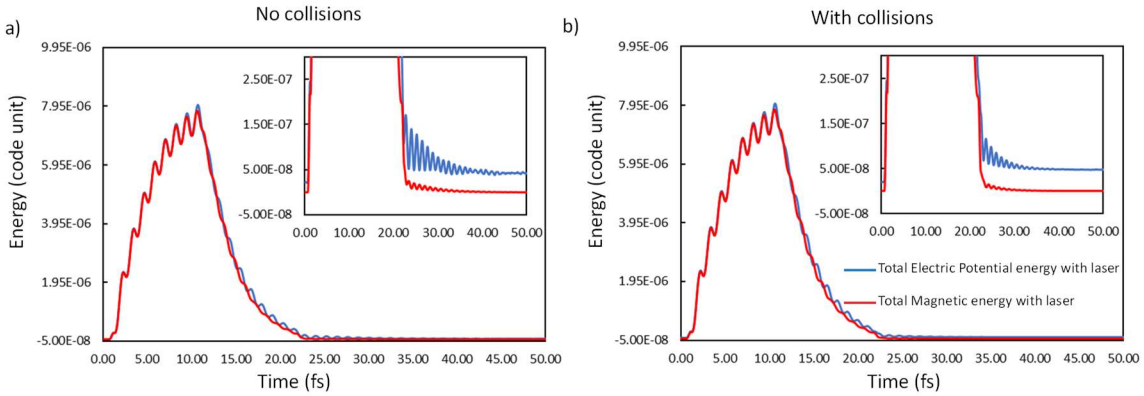

Figure S2. Time-dependent energy components without subtraction of the laser field, integrated over all simulation box. Insets are the same plots with zoomed-in y-axis.

[1] P. B. Johnson and R. W. Christy, *Phys. Rev. B*, 1972, **6**, 4370.

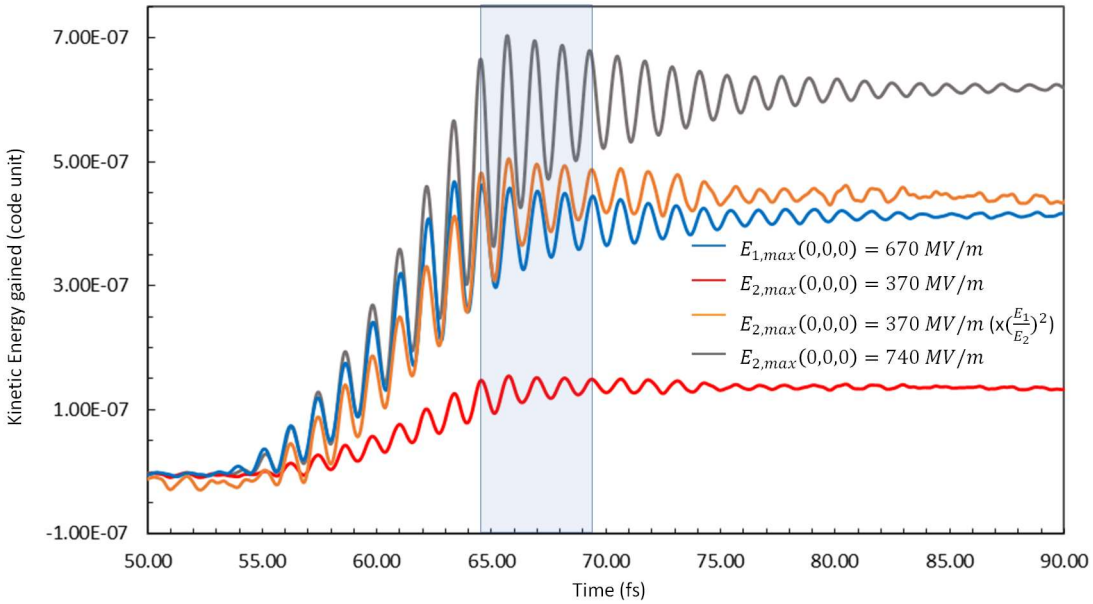

Figure S3. Benchmarking the kinetic energy gained for different excitation field strengths. The electric field amplitude of the laser at the center of the nanorod was set as 740 MV/m (gray), 670 MV/m (blue) and 370 MV/m (red). First, the blue and red plot show similar behaviour and a similar oscillation cycle pattern during damping. For better comparison, the latter is magnified (orange) by the ratio between the laser power $\frac{P_1}{P_2} \approx \left(\frac{E_{1,max}}{E_{1,max}}\right)^2 = 3.28$.

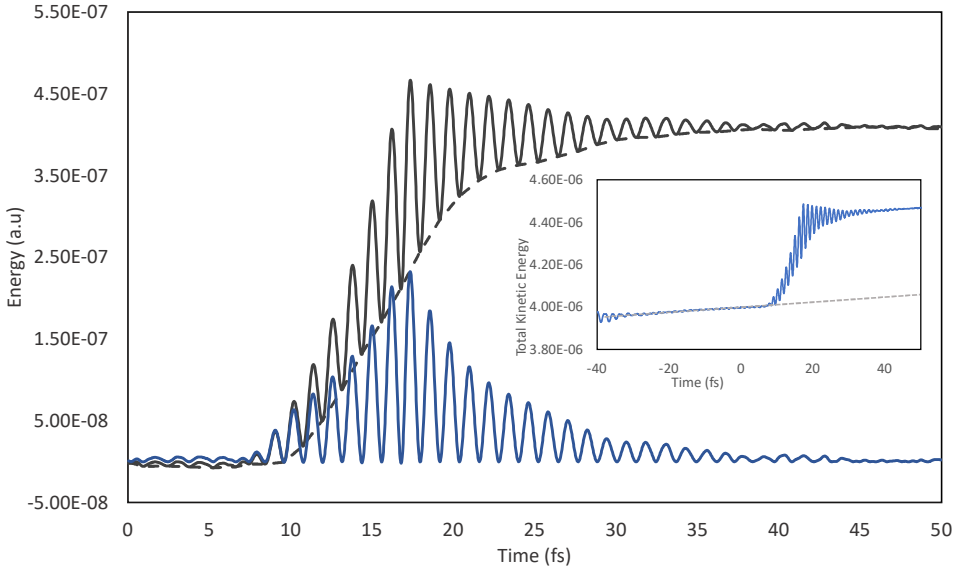

Figure S4. Extracting the kinetic induction energy from the total kinetic energy gain. The kinetic induction energy curve (blue) was obtained by extracting the oscillation part of the total kinetic energy gain (full black) from the baseline (dashed black). The inset shows that the total kinetic energy gain was obtained from the total kinetic energy by subtracting a straight line fitted before excitation (dashed grey line).

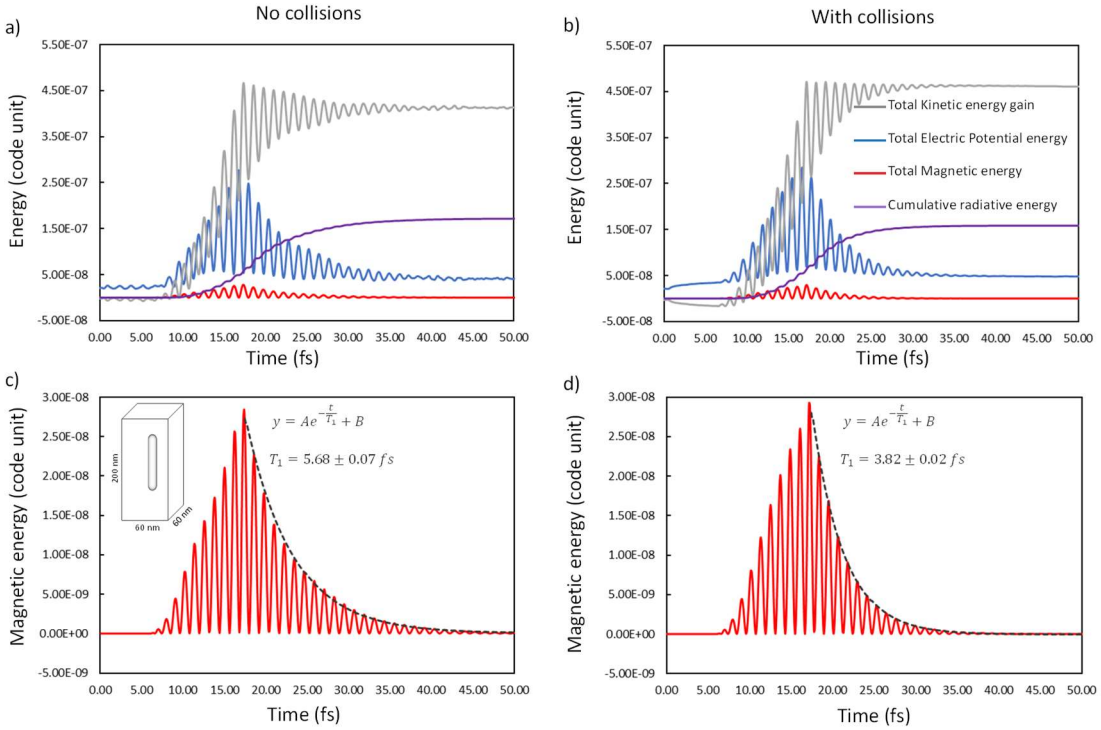

Figure S5. Time-dependent energy components and calculation of the population relaxation time T_1 and dephasing time T_2 for the no-collisions and with-collisions cases. (a, b) Time dependent kinetic energy gain, electric energy, magnetic energy and cumulative radiative energy in collisionless (a) and collisional (b) case. The total kinetic gain was obtained as $\Delta KE = KE(t) - KE(0)$, then subtracted with a straight line to compensate for the self-heating effect of PIC obtained from initial redistribution[2] (see Movie M1). Electric and magnetic energy are integrated in a 60×200×60 nm^3 box surrounding the nanorod. The cumulative radiative energy is taken as the time-space integration of Poynting vectors on a sphere $r = 500\,nm$ from the center of the rod, corresponding to the instantaneous radiative power in Figure 2c. (c,d) Calculation of the population relaxation time T_1 by fitting the time-dependent magnetic energy with the damped harmonic oscillator model for the collisionless (c) and collisional (d) case. The fitting function is $y = Ae^{-t/T_1} + B$. The magnetic energy is selected for deriving the dephasing time as it shows the clearest signal, while the kinetic energy and potential energy include noise from hot electrons that interferes with the oscillation amplitude. The dephasing time is then calculated via $T_2 = 2T_1$ as explained in the main text and consolidated in Figure 3a.

[2] P. Y. Lai, T. Y. Lin, Y. R. Lin-Liu, S. H. Chen, *Physics of Plasmas*, 2014, **21**, 122111

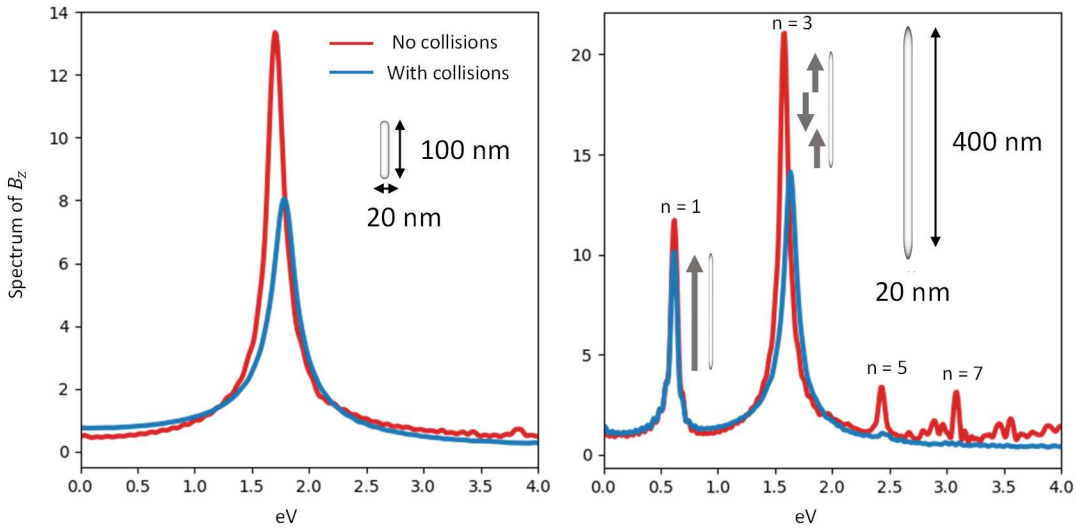

Figure S6. The scattering spectra shown as insets in Figure 3(c) are calculated by integrating the real part of Poynting vector in the frequency domain $\boldsymbol{S}(\omega)$ 500 nm away from the nanorod. $\boldsymbol{S}(\omega) \sim \boldsymbol{E}(\omega) \times \boldsymbol{B}^*(\omega)$ with $\boldsymbol{E}(\omega)$ and $\boldsymbol{B}(\omega)$ obtained from the Fourier transform of $\boldsymbol{E}(t)$ and $\boldsymbol{B}(t)$ during plasmon damping from $t = 18$ to $t = 50$ fs. These scattering spectra show a mismatch in the resonance frequency; both are plotted in the left panel. This is probably due to the interaction between the transverse oscillation and longitudinal oscillation in the collisionless case in Figure 3c. The effect is less significant with increasing aspect ratio, as shown in the right panel for the near-field spectrum of a 400 nm long nanorod. Both rods are excited with a 10-fs laser pulse at 1.7 eV. The near-field spectra are taken after excitation has ended. For the 400 nm long nanorod, two bright modes can be observed both for collisional and collisionless case, at about 0.6 eV for the dipole mode and at 1.6 eV for the quadrupole mode, while n = 5 and n = 7 are suppressed in the collisional case. The mismatch is not significant for the first resonance peak, but increases with the harmonic order of the mode. At higher harmonic mode, the oscillation length of the plasmon bunches gets more localised, making the effect of mean free path more significant.

However, it should be noted that this binary collision model is designed for plasmas. Therefore, further optimization of the collision rate (or Coulomb log[3]) is required for more realistic models. Here, we use the Coulomb log = 2, calculated from the density and temperature of the electron plasma based on the approach by Nanbu and Yonemura[4].

From the formulation by Lee and More[5] using the non-degenerate limit, the electron-electron collision relaxation time can be estimated as:

$$\tau = \frac{3}{4}\frac{\sqrt{m}}{\sqrt{2\pi}}\frac{(kT)^{3/2}}{(Z^*)^2 n e^4 ln\Lambda}\ (cgs) \approx 0.04 fs$$

with $kT \sim E_F = 5.53\ eV$, $n = 5.9 \times 10^{28} m^{-3}$, $Z^* = 1$ and $ln\Lambda = 2$ obtained from the simulation.

Future studies revealing the effect of electron dynamics on the spectral response of plasmons using PIC will be valuable.

[3] F. Pérez, L. Gremillet, A. Decoster, M. Drouin and E. Lefebvre, *Phys. Plasmas,* 2012, **19**, 083104.
[4] K. Nanbu, S. Yonemura, *J. Comput. Phys.*, 1998, **145**, 2, 639-654.
[5] Y. T. Lee and R. M. More, *Phys. Fluids.,* 1984, **27**, 1273.

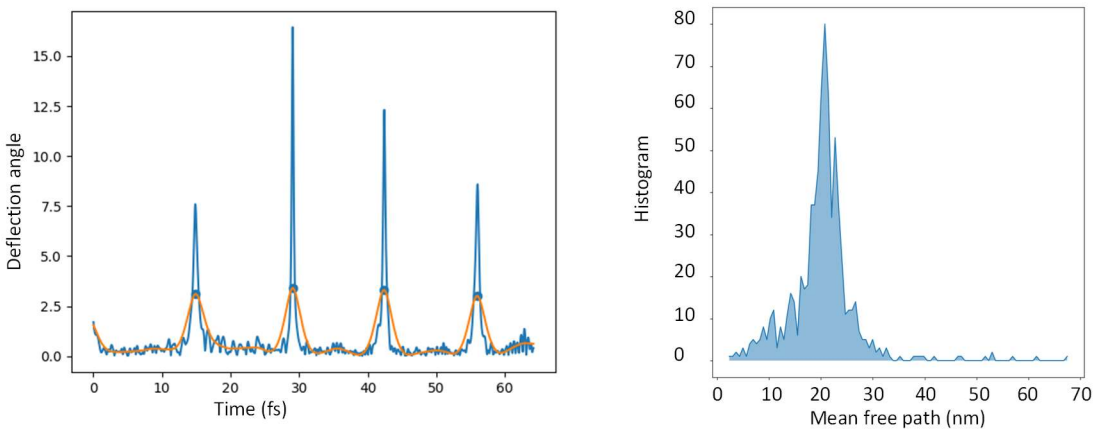

Figure S7. In the collisionless case, we can estimate the mean free path of the electrons due to surface scattering by tracking the deflection angle of the electron trajectory. Left: an example of scattering events detection by detecting peaks in the deflection angle curve (blue curve) after a low-pass filter (orange curve) and peak detection (blue circles) using the Scipy[6] package. The mean free path of each particle is calculated from the distance travelled between two consecutive scattering events. In this way, the mean free path of 754/1000 sampled particles was calculated. Right: a histogram of the mean free path of the sampled particles, giving an average mean free path of 20.26 nm.

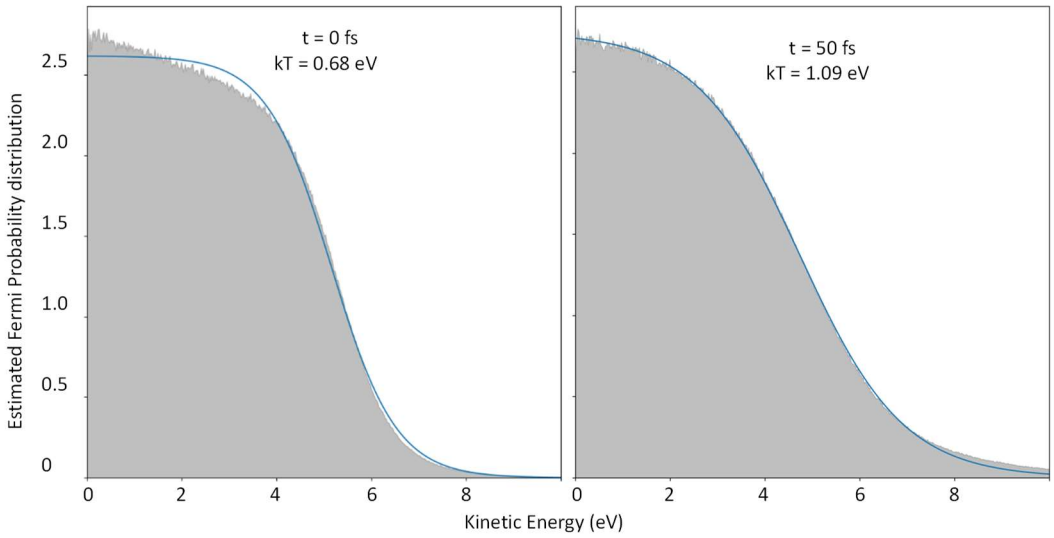

Figure S8. Electron temperature estimated from the electron energy distribution with Fermi-Dirac statistics. To quantitatively extract further information from the electron energy distribution in Figure 3b, we attempt to estimate the temperature of the electron gas before and after plasmon damping by fitting the electron energy distribution with the Fermi-Dirac model:

$N(E) = g(E)f(E)$, where $g(E)$ is the parabolic density of state, $f(E) = \frac{a}{e^{\frac{E-E_F}{kT}}+1}$ is the probability based on Fermi-Dirac statistics, a, E_F and kT are the fitting parameters. The fitted line of $f(E)$ is plotted in blue before (left) and after (right) excitation, corresponding to Figure 3b-I and Figure 3b-IV. There are two reasons for the surprisingly high electron temperatures. The first reason is the self-evolving electron energy distribution due to the initialisation as visualised in Movie M1. Secondly,

[6] https://www.scipy.org/

electron-phonon interaction is not included in this simulation as the timescale of such interaction is in picoseconds[7], which is much larger than the plasmon decay time considered in this study. The increase in electron gas temperature after plasmon damping is comparable with previous estimations by Saavedra *et al*. (2016)[8] through the temperature-dependent electron occupancies, guaranteeing energy conservation during electron-electron scattering.

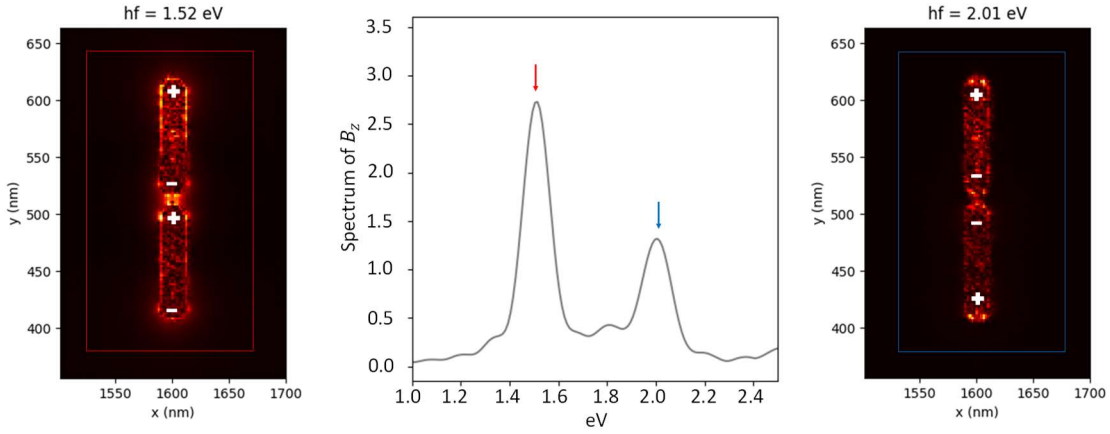

Figure S9. Nanorod dimer excited by an electron beam. The PIC method is not limited to single particles, but can also be used to simulate more complex structures, such as nanorod dimers. Here, two nanorods with the same geometry as Figure 2a are placed 10 nm apart. The system is excited by a fast-moving charge Q = -1000e moving at $v = 0.5c$ in the x-direction, 4 nm off the top end of the upper nanorod as described earlier[9]. Center panel: a Fourier transform of the near field shows two resonance peaks, at 1.52 eV and at 2.01 eV, corresponding to two oscillation modes depicted in the left and right maps, respectively. The maps show the spatial distribution of the electric field strength at resonance frequencies by taking the real part of $E_x(\omega, z = 0)$ and $E_y(\omega, z = 0)$ on the z-plane of symmetry. The spectrum is calculated from $B_z(\omega, z = 0)$.

[7] J. -Y. Bigot, V. Halté, J. -C. Merle, A. Daunois, *Chem. Phys*., 2000, **251**, 1-3, 181-203.
[8] J. R. M. Saavedra, Asenjo-Garcia A., de Abajo F. J. G., *ACS Photonics*, 2016, **3**, 9, 1637-1646.
[9] W. J. Ding, J. Z. J. Lim, H. T. B. Do, X. Xiong, Z. Mahfoud, C. E. Png, M. Bosman, L. K. Ang and L. Wu, *Nanophotonics*, 2020, **9**, 3303-3313.

Description of the Supplementary Movies

Movie M1. Self-evolving electron energy distribution from Fermi-Dirac initial momentum distribution at Fermi energy 5.53 eV. The system is started as neutrally charged with electrons and ions at identical positions but self-evolves as the electrons spill outside of the ions boundary. Within a few femtoseconds, the system stabilizes, resulting in thermalisation and deviation from the initial distribution. The issue may be solved in future work with initialising electrons at equilibrium density distribution obtained by solving for a self-consistent potential with Fermi-Dirac distribution as shown in 1D for the Vlasov simulation[10]. Because of the non-equilibrium initialisation, we start the laser excitation after about 40 fs, when the initial redistribution has almost stabilised.

Movie M2. v_y distribution from t = 16.9 fs to t = 20.2 fs during plasmon oscillation. The Fermi velocity is $1.4 \times 10^6\ m/s$.

Movie M3. Difference between the v_y distribution and the average distribution from t = 16.9 fs to t = 20.2 fs during plasmon oscillation. The average distribution is the mean of all calculated distributions from t = 18.6 fs to t = 19.9 fs.

Movie M4. 1000 random electrons in phase space (collisionless plasma).

Movie M5. 1000 random electrons in real space on the x-y plane (collisionless plasma).

Movie M6. 1000 random electrons in real space in 3D (collisionless plasma).

Movie M7. Poynting vectors on $z = 0$.

Movie M8. Distribution of the electron kinetic energy during excitation and damping (collisionless plasma).

Movie M9. Tracking two sampled electrons scattering at the surface. The color bar represents the kinetic energy of the particles normalised to the Fermi energy. The grey stream plot and black arrows represent the electric field lines and momentum in x-y plane, respectively. The solid black curve marks the position of ion background surface. Both particles participate in the oscillation until they reach the surface around t = 18 fs.

Movie M10. Tracking a few electrons mainly traveling in y-direction on the x-y plane before surface scattering. The color bar represents the kinetic energy of the particles normalised to the Fermi energy. The solid black curve marks the position of the ion background surface.

[10] G. Manfredi and P.-A. Hervieux,. *Phys. Rev. B*, 2004, **70**, 201402(R)